



RESEARCH LETTER

10.1002/2015GL063063

Key Points:

- Largest waves measured under ice cover in the Arctic
- High-resolution, coupled wave-ice models are required for accurate predictions
- Nonlinearly enhanced waves may lead to initial ice breakup

Supporting Information:

- Texts S1–S5, Figures S1–S5, and Tables S1 and S2

Correspondence to:

C. O. Collins,
Tripphysicist@gmail.com

Citation:

Collins, C. O., III, W. E. Rogers, A. Marchenko, and A. V. Babanin (2015), In situ measurements of an energetic wave event in the Arctic marginal ice zone, *Geophys. Res. Lett.*, 42, doi:10.1002/2015GL063063.

Received 7 JAN 2015

Accepted 27 FEB 2015

Accepted article online 3 MAR 2015

In situ measurements of an energetic wave event in the Arctic marginal ice zone

Clarence O. Collins III¹, W. Erick Rogers², Aleksey Marchenko³, and Alexander V. Babanin⁴

¹ASEE Postdoctoral Fellow, Naval Research Laboratory, Stennis Space Center, Hancock County, Mississippi, USA,

²Oceanography Division, Naval Research Laboratory, Stennis Space Center, Hancock County, Mississippi, USA, ³Department of Arctic Technology, University Center in Svalbard, Longyearbyen, Norway, ⁴Centre of Ocean Engineering, Science and Technology, Swinburne University of Technology, Hawthorn, Victoria, Australia

Abstract R/V *Lance* serendipitously encountered an energetic wave event around 77°N, 26°E on 2 May 2010. Onboard GPS records, interpreted as the surface wave signal, show the largest waves recorded in the Arctic region with ice cover. Comparing the measurements with a spectral wave model indicated three phases of interaction: (1) wave blocking by ice, (2) strong attenuation of wave energy and fracturing of ice by wave forcing, and (3) uninhibited propagation of the peak waves and an extension of allowed waves to higher frequencies (above the peak). Wave properties during fracturing of ice cover indicated increased groupiness. Wave-ice interaction presented binary behavior: there was zero transmission in unbroken ice and total transmission in fractured ice. The fractured ice front traveled at some fraction of the wave group speed. Findings do not motivate new dissipation schemes for wave models, though they do indicate the need for two-way, wave-ice coupling.

1. Introduction

The marginal ice zone (MIZ) is the transition zone between continuous ice cover (so-called pack ice) and the open oceans. The MIZ is highly dynamic with coupled interactions between the ice floes and open ocean processes. Interactions between wind-generated ocean surface waves and sea ice have been a focus of research for some time (e.g., see the reviews by *Wadhams* [1981], *Squire et al.* [1995], and *Squire* [2007]). The majority of these studies have been theoretical in nature, based on measurements in the laboratory, or based on remote sensing observations. To complement these studies, more analysis of past in situ measurements in the MIZ is beneficial, particularly for planning future field studies.

Long waves may propagate relatively unhindered through ice. It is not uncommon for vessels to experience swell events, even deep into ice fields, but very few of these events have been reported over the years [e.g., *Robin*, 1963; *Liu and Mollo-Christensen*, 1988; *Asplin et al.*, 2012], and none of these report large waves (e.g., greater than 3 m). The scarcity of in situ wave measurements in the MIZ is perhaps unsurprising considering the proportion of global ship traffic that occurs in these areas. Very large waves routinely occur in the Antarctic due to the nearly unlimited fetch, yet measurements of large waves in the MIZ are nonetheless rare. Very recently, *Doble and Bidlot* [2013] (henceforth DB13) reported buoy measurements of very large waves in the Antarctic MIZ. Other much less energetic (though still of interest) measurements have also been reported [e.g., *Fox and Haskell*, 2001; *Meylan et al.*, 2014]. The Arctic fetch (i.e., the spatial potential for wave development) is limited by ice cover (see the inset in Figure S5 of the supporting information), so measurement of large waves is rarer still [*Thomson and Rogers*, 2014]. Several remarkable studies have been made in less energetic wave environments [e.g., *Hunkins*, 1962; *Liu et al.*, 1991; *Marko*, 2003].

Mariners have long known that wave energy diminishes as they navigate into ice, and many have witnessed swell propagate deep (distances of 2 to 4 orders of magnitude greater than the characteristic wavelength) into the ice. Research has focused on several effects of ice cover on incoming waves: change in dispersion relation [e.g., *Hunkins*, 1962; *Liu et al.*, 1991; *Fox and Haskell*, 2001] and other radiative effects such as reflection, transmission [*Goldshstein and Marchenko*, 1989; *Fox and Squire*, 1994], scattering, refraction, and attenuation [*Squire et al.*, 1995; *Perrie and Hu*, 1996; *Marchenko and Voliak*, 1997; *Liu and Mollo-Christensen*, 1988; *Squire and Williams*, 2008]. The wave effects on ice are mostly mechanical in nature: flexing and fracturing of continuous ice and floes, calving of ice edges, convergence or divergence of ice fields, and forcing collisions between floes [*Wadhams*, 1981; *Squire*, 2007, and references within]. Ice is often heterogeneous in nature and varied in form which greatly impacts wave-ice interaction [e.g., *Campbell et al.*, 2014].

Of special interest is the fracturing and convergence of ice floes under the influence of swell because this represents a possible feedback loop between air, sea, and ice [Asplin *et al.*, 2012; Thomson and Rogers, 2014; Asplin *et al.*, 2014]. On the macroscale (e.g., seasonal), action of wind on the open sea generates waves; these waves contribute to the fracturing of ice through mechanical strain (i.e., creeping and bending). By increasing the surface area of individual ice floes, this fracturing accelerates melting. The newly ice-free regions increase the area of open sea (i.e., fetch), in turn allowing larger waves to form and break up more ice. It is thought that this process will become more important as the warming climate reduces the extent of perennial Arctic ice cover [Squire, 2007; Squire *et al.*, 2009; Khon *et al.*, 2014]. On the microscale (time scale of hours), we propose that large-wave events fracture ice, creating an ice cover that permits the passage of a larger fraction of the wave energy (as documented by DB13), leading to more wave energy further into the ice, and further fracturing of the ice, until an equilibrium (between wave strain and ice strength) is reached or the event ends, and the event-induced migration of the MIZ toward the interior is halted.

Traditionally, sea ice has been treated simplistically in the spectral models that are used for routine hindcasting and forecasting of surface waves, such that the MIZ is treated as either open water or impermeable (as land) based on an ice concentration criterion [Tuomi *et al.*, 2011]. This was improved somewhat by Tolman [2003] using a cell-wise partial blocking of energy flux, scaled by ice concentration. Wave-ice interaction remains an area of wave modeling which is ripe for progress. More recently, efforts have been made to incorporate the effect of ice into the physics of these wave models [DB13; Rogers and Orzech, 2013; Rogers and Zieger, 2014; Tolman and the WAVEWATCH III® Development Group, 2014]. Wave energy can be either scattered and reflected (conservative processes) or dissipated (a nonconservative process). Either causes a reduction of wave energy along the main axis of propagation. With respect to dissipation, there are a few theoretical paradigms, any of which may be valid under certain circumstances owing to the varied nature of ice floes. Two that have been proposed are dissipation through turbulence generated beneath ice [Liu *et al.*, 1991] and dissipation through an effective viscosity of the ice cover [Keller, 1998; Newyear and Martin, 1999; Wang and Shen, 2010]. In the case of the implementation in the WAVEWATCH III® model [Rogers and Orzech, 2013; Rogers and Zieger, 2014; Tolman and the WAVEWATCH III® Development Group, 2014], the new formulations remained uncalibrated except in the most gross sense; and therefore, field studies with detailed wave measurements (such as the one described herein) are seen as an opportunity to perform such calibrations. The data set of the present study, though not ideally suited for such calibration work, does benefit our understanding of wave-ice interaction in terms of model requirements (see section 4).

Some of the aforementioned reports arose from data of opportunity, that is to say the field experiments were not designed for wave measurements, and the same may be said for our study. To help fill the gap of in situ observations of wave-ice interaction, we present the largest waves measured in the Arctic under significant ice cover (section 3) and, during the breakup phase (section 3.2), closely examine wave properties and infer ice quality. These measurements are compared with results from a spectral wave model (section 3), and the requirements for accurate wave prediction are discussed (section 4). In addition, the possible role of nonlinear wave focusing during ice breakup is discussed (section 4.1).

2. Methods

The R/V *Lance* is a former fishing vessel, converted for research and expedition and operated by the Norwegian Polar Institute. This particular cruise was organized for the field works section of the University Center in Svalbard's course concerning drifting ice in the Barents Sea. The R/V *Lance* is 60.8 m in length by 12.6 m in breadth. The location, including vertical position, of the vessel was recorded by an onboard Seapath 200 GPS system at 1 Hz. The accuracy of the vertical position was greater of 0.05 m or 5% (defined in the Seapath 200 technical documentation). Using this record, the ship velocity was determined from tracking the location and the sea surface elevation, η , from detrending the vertical position. Treating the vessel as a surface following buoy whose dimensions act as a low-pass filter to the signal from the ambient sea surface spectrum, 1-D frequency spectra were calculated from 1 h records of η . In theory, if the vessel is stationary, waves with lengths at least twice its dimensions may be accurately resolved assuming a perfect response. This implies a minimum wavelength (maximum frequency assuming linear dispersion relation) of 121.6 m (0.113 Hz) for waves approaching head on and 25.2 m (0.249 Hz) for waves approaching the broadside.

Since R/V *Lance* is most effective in measuring relatively low frequency wave energy, we will compare an equivalent low-frequency height by integrating the 1-D wave spectrum, $S(f)$, in analogy to significant wave height, but with an upper frequency bound

$$H_{low} = 4 \left[\int_{0 \text{ Hz}}^{0.12 \text{ Hz}} S(f) df \right]^{1/2}$$

Later in the paper, we discuss wave groupiness (section 4.1). We calculated two associated metrics: the so-called Benjamin-Feir Index, BFI [Janssen, 2003], and the relative spectral width parameter, ν [Babanin and Soloviev, 1998]:

$$BFI = 2\sqrt{2\pi}k_p n_1^2 m_0^{-3/2}$$

$$\nu = n_0^1 [f_p S(f_p)]^{-1}$$

where f_p is the frequency at the peak (i.e., most energetic region) of the spectrum (aka peak frequency) and k_p is determined by the deep water linear dispersion relation, $f_p = \sqrt{gk_p}/2\pi$. The usual zeroth-order spectral moment is m_0 , and n is a modified spectral moment as follows:

$$m_j = \int_0^{f_{max}} f^j S(f) df$$

$$n_j^k = \int_{0.5f_p}^{2f_p} f^j S(f)^k df$$

We do not compare these parameters with a model, hence, the spectral bounds have been relaxed to include higher-frequency waves. Wave measurements from a vessel underway present a problem for interpretation of the signal. This is because the forward speed, with no changes in velocity or heading, enters into the dispersion relation as an extra term:

$$f = \left(\sqrt{gk} - |k||V|\cos\alpha \right) / 2\pi$$

This is the well-known Doppler shift [e.g., Hanson *et al.*, 1997] which changes the frequency, measured in the ship frame of reference, according to the (1) relative angle between the wave propagation direction and the ship heading, α , and the (2) product of the magnitudes of the ship velocity, V , and wave number, k (derived from the intrinsic frequency). To avoid this issue, analysis was confined to a period when the ship speed was below 3 m/s (note that the frequencies considered in H_{low} have phase speeds > 13 m/s).

A nested run of SWAN (“Simulating WAVes Nearshore”) [Booij *et al.*, 1999] was performed as part of the analysis of this wave event. The outer computational grid was defined from $[-24^\circ\text{E}, 66^\circ\text{N}]$ to $[53^\circ\text{E}, 79^\circ\text{N}]$ with $\sim 1/3^\circ$ resolution and the inner computational grid from $[15^\circ\text{E}, 74^\circ\text{N}]$ to $[30^\circ\text{E}, 78^\circ\text{N}]$ with $\sim 1/10^\circ$ resolution. The model topography was from ETOPO2 [National Geophysical Data Center, 2006], and the 10 m wind vectors were obtained from archives of the U.S. Navy’s operational analyses (Navy Operational Global Atmospheric Prediction System) [Hogan and Rosmond, 1991]. SWAN was run without any representation of the ice, though operational analyses from the Navy’s Polar Ice Prediction System (PIPS) [Van Woert *et al.*, 2004] were used to give a large-scale, spatial overview of the concentration of sea ice. PIPS was updated once per day at noon UTC. For local, qualitative inferences of ice conditions, we utilized the first-hand account of author A.M. and bow-oriented photographs captured hourly.

3. Results

3.1. Phase 1—Wave Blocking by Solid Ice

Phase 1 is marked in red in Figure 1 and spans the time period from 2 May 2010 15:00–20:15 UTC. On 1 May 2010, a low-pressure system over northern Europe moved northeast and strengthened over the Barents Sea on 2 May 2010. During this time, field work required R/V *Lance* to moor to pack ice about 75 km north northeast of Hopen Island (Svalbard, Norway). Visual ice observations indicated continuous, pack ice with relatively flat surfaces covered by snow. Ridge sail heights did not exceed 1 m, and the ice thickness was typical for this area at this time of year (~ 0.5 – 0.6 m). The rigid structure of the ice can be seen in Figure 1d. Since there was no ice representation in SWAN, SWAN predicted a gradual increase of wave height from

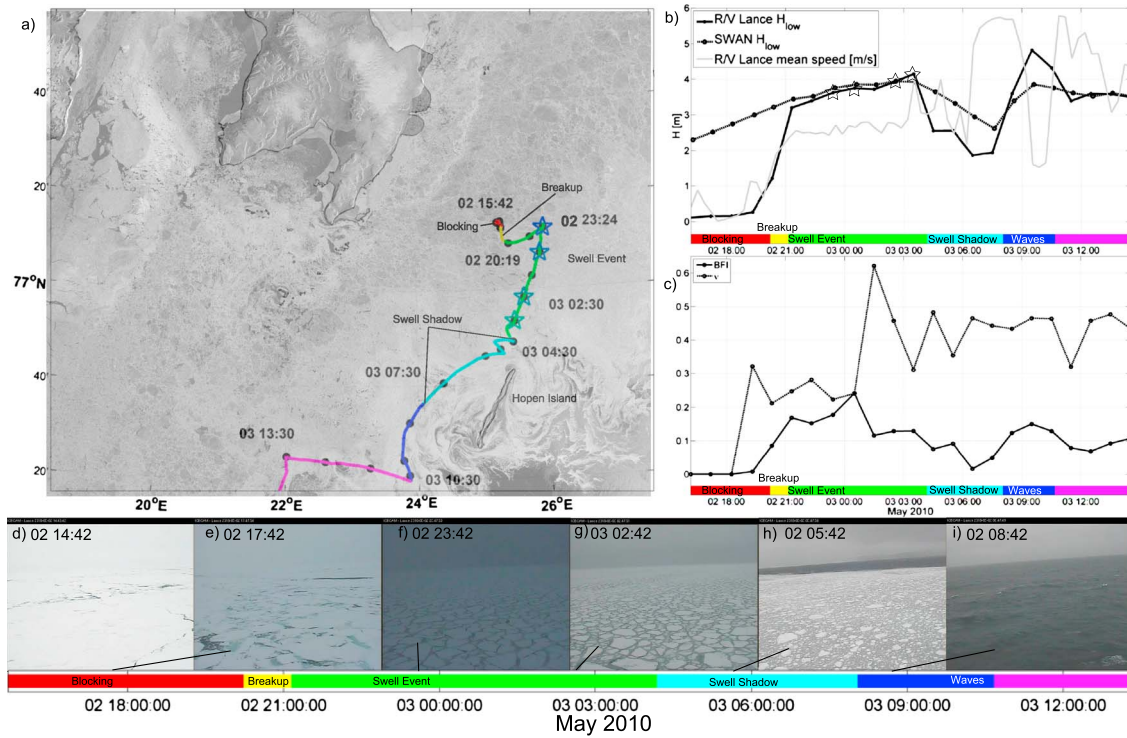


Figure 1. (a) Map of southern Svalbard in the top left and Hopen Island in the bottom right. The ship track is in color corresponding to different phases of wave interaction (red: wave blocking by ice, yellow: arrival of waves and breakup of the ice, green: swell event at full energy allowing higher frequencies with time, cyan: the swell shadow of Hopen Island, blue and purple: after the swell shadow). Black dots correspond in space to the black dots in the time series. Stars (and colors) correspond with the spectra shown in Figure 3. The background is superimposed with an advanced synthetic aperture radar image captured on 1 May 2010 09:45:38 UTC on the Envisat satellite operated by European Space Agency and provided by Benjamin Holt at the Jet Propulsion Laboratory. (b) Time series of H_{low} as measured by R/V *Lance* (black solid line) and predicted by SWAN (black dashed line) and the ship velocity (grey solid line). Stars correspond with the spectra shown in Figure 3. (c) BFI (black solid line) and v (black dashed line). (d–i) Select photographs from the ship show local sea ice state. A color bar, corresponding to the colors of ship track, is located at the bottom of each time series for convenience. The phases of wave interaction are labeled.

around 1 m at ~09:00 to 4 m at ~21:00, during which time the pack ice was, in reality, blocking almost all incoming wave energy. The first waves were measured at ~19:40 as an isolated wave group (see Figure 2), the central wave height of which was 0.9 m. Soon after, newly formed cracks in the ice were discovered, and it was deemed too dangerous to continue field operations. It is probable that wave energy was transmitted into the ice as flexural-gravity waves, of amplitude too small for the ship to measure reliably, but which were responsible for the formations of the cracks in the ice.

3.2. Phase 2—Ice Breakup and Transition

Phase 2 is marked in yellow in Figures 1 and 2. At ~20:15, less than an hour following the isolated wave group, the ship again encountered small waves. Over the course of the next hour, the cracked ice gave way and broke into smaller floes, and the observed waves, which were initially under 1 m, very quickly became 4 m swell. Figure 2e shows the time series of η and photographs of the ice during the transition. The ice is largely unchanged between Figures 2a and 2b. In Figure 2c, the ice appears slightly more homogenous while still retaining larger floes, while in Figure 2d, the ice is clearly broken into smaller, more uniform, floes. The waves during the transition period have a grouped (modulated) structure in Figure 2, which manifests as elevated BFI and lower v in Figure 1c. At the end of this 1 h transition period, the H_{low} matched the prediction from SWAN.

3.3. Phase 3—Continued Fracturing

Phase 3 is marked in green in Figures 1 and 2. The ship continued to measure large swell over the next 7 h as it slowly steamed through the MIZ headed for protected waters behind Hopen Island. Simple analysis of Figure 1g (see supporting information) showed that the peak wavelength (~200 m) was much longer than the typical floe size (~5–10 m). H_{low} from SWAN agreed nearly perfectly with the ship measurements during

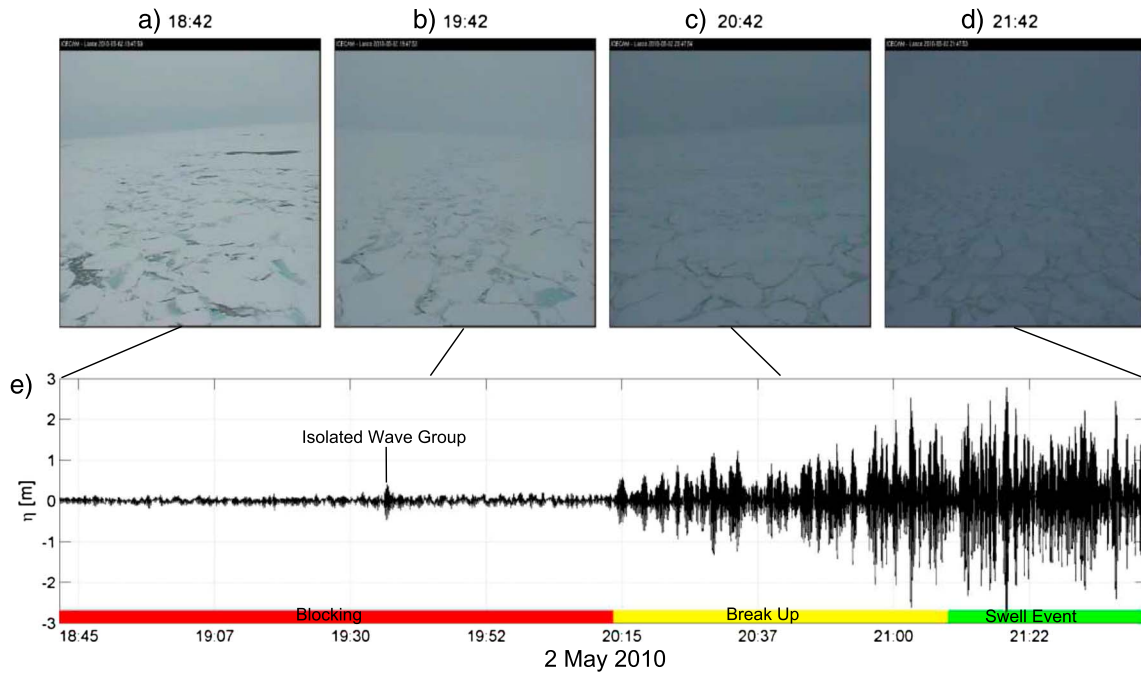


Figure 2. Time series of sea surface elevation, η , derived from GPS on R/V Lance and corresponding photographs of the ocean surface before, during, and after the ice breakup.

this period, implying that the ice had little or no effect on the waves measured by the ship. The measured spectra in Figure 3, which correspond to the stars in space and time in Figures 2a and 2b, respectively, show that there was a continuous increase in energy at frequencies above the spectral peak. At ~04:00 on 3 May 2010, the ship reached the swell shadow of Hopen Island and allowed for breakfast before steaming onward, at an increased pace, to the south. The vessel again encountered large waves at ~08:00 (seen as blue in Figure 1) as it exited the swell shadow headed east.

4. Discussion

4.1. Groupiness

The waves which were responsible for the initial breakup of the pack ice were “groupy,” meaning the wave energy arrived in discrete packets or groups (also referred to as “sets,” “beats,” or “envelopes”). This is evident in the time series of η in Figure 2 and is corroborated by spectral parameters BFI and ν in Figure 1c. BFI is

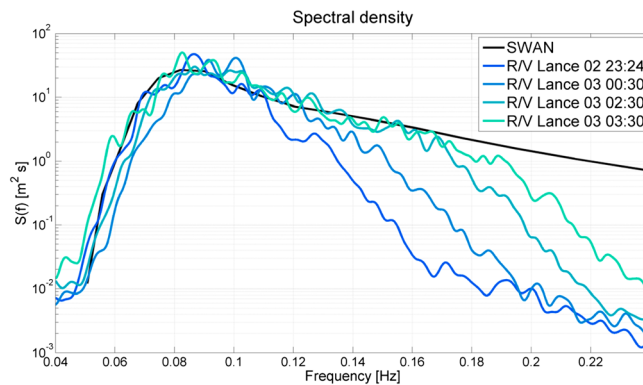


Figure 3. The evolution of $S(f)$ over the course of 5 h as the ship encountered smaller ice floes. The first spectra is shown in dark blue, and later spectra transitioning to aqua. SWAN spectra at this time, with no ice representation, is shown in black for reference.

the ratio of nonlinearity to dispersion, and dispersion is related to the spectral width. From Figure 3, it is evident that the spectra were filtered (more on this follows below), effectively decreasing the spectral width which manifest as a larger (smaller) BFI (ν) near the transition (phase 2). This indicates that the wave system may have been subject to modulation instability (MI) [Benjamin and Feir, 1967; see also Yuen and Lake, 1982]. It was shown by Liu and Mollo-Christensen [1988] that monochromatic waves more quickly destabilize into groups when the sea surface is under high compression stress (i.e., ice cover) than over the

open ocean. If this is true, the nonlinear focusing of wave energy via MI may possibly explain how large waves are able to penetrate more deeply into ice cover. A feedback mechanism is possible: the compact nature of the (ice covered) sea surface provides a medium which enhances the self focusing of the waves (i.e., MI), these waves, in turn, increase the strain which leads to the initial breaking of the ice, broken ice allows the waves to travel more deeply into covered ice. In this way, nonlinear wave trains lead the advance into the unbroken ice field. After the initial passage of wave groups, ice no longer provides the type of stress which leads to enhanced self focusing, nor does it inhibit freely propagating linear waves in its fractured state. This transition period is about 1 h in length for our wave event. This represents a new and potentially important mechanism for rapid ice breakup.

This theory, however, must be tempered by uncertainties in the explanation. Most significant is the exact nature of the dispersion relation (important for the calculation of *BFI* via steepness) in the MIZ. In ice, the dispersion relation has additional dependencies on ice properties including thickness, elastic modulus, compression stress, and viscosity. The amount of compression stress assumed in *Liu and Mollo-Christensen* [1988] may not be representative of typical sea ice conditions [e.g., *Hibler*, 1979, also see *Timco and Weeks*, 2010]. The detailed ice properties during phase 2 in this study are unknown; furthermore, the exact nature of the dispersion relation in ice is a matter of contention for which there is little observational evidence. Certainly, much more research is needed to establish the importance of such a mechanism.

4.2. Ice as a Low-Pass Filter

Figure 3 shows the evolution of wave spectra with time. Measured spectra are shown in color indicating the time, and a spectrum from SWAN is shown in black as a “no ice” reference. The spectral density changes little below the spectral peak, but above the peak, more and more energy was being detected as time progressed. This observation is similar to that of a low-pass filter in which the cutoff frequency is increasing with time. We suggest that the ice field acted as the filter [*Marko*, 2003]. As evidenced in the photographs in Figures 2 and 3, the ice field was characterized by smaller floes as time passed. The smaller dimensions of the floes allowed higher-frequency waves to propagate. Similar features may be seen in the observations of *Robin* [1963, Figures 7 and 8].

The smaller floe diameters may have been a result of wave action (temporal change in ice structure) or the ship moving toward the open water through the MIZ (spatial change in ice structure). The satellite image in Figure 1a and the ice concentrations from PIPS (see Figure S5 of the supporting information) suggest the latter possibility. In all likelihood, it was a combination of nonstationary and nonuniform ice contributing to the varied ice characteristics observed by the moving ship.

4.3. Fractured Ice Front

We hypothesize that there was a front separating nearly solid pack ice and fractured ice. This front, driven by wave action, was traveling deeper into the ice field. Eventually, this front crossed the position of the ship, the time at which it first encountered the wave event. SWAN was used to estimate the delay of swell event to be ~12 h. PIPS was used to estimate the distance from the position of R/V *Lance* to the closest ice edge in the direction of wave propagation to be ~200 km. With these two quantities, the speed of the front is estimated to have been roughly 4.5 m/s, which happens to be about half the wave group velocity. The fact that the estimated speed of the fractured ice front was some significant fraction of the group speed means the nature of the ice field was changing (in time and space) on scales similar to those which characterize the peak waves.

4.4. Implications for Ice Implementation in Spectral Wave Models

The results presented here have implications for spectral wave models, although, being a case study, the generality of the implications is not known. There is limited evidence that large waves behave differently in ice [*Kohout et al.*, 2014]; as such, it is unclear if this study represents typical wave-ice interactions. *Kohout et al.* [2014] claim that wave heights greater than 3 m (for a certain wave period) are linearly attenuated by ice, whereas waves of heights less than 3 m are exponentially (i.e., more strongly) attenuated. Our results also support less attenuation for larger waves. In fact, the close agreement with the model (keeping in mind there is no ice representation in the model) implies there is negligible wave attenuation at the peak frequencies by fractured floes. This is in agreement with results of DB13. Our observations indicate wave-ice interaction with binary behavior, where peak waves are completely blocked (i.e., 100% dissipation), then completely passed (i.e., zero dissipation) with a very short transition time ($O(1\text{ h})$). This type of behavior has important implications for wave modeling. If the wave model was “aware” of the location of the solid ice, it could well

predict the wave conditions by not allowing energy to propagate into that region. We have shown that it may be possible for the location of the solid ice edge to move at some significant fraction of the wave group speed. Hence, the wave model would not perform well with information from routine ice products which are low resolution in space ($O(10\text{ km})$) and sparse in time (updated once per day). It is also not clear that ice concentration would necessarily be different for unbroken and broken ice, so perhaps, a new type of ice product is needed. In essence, accurate wave prediction would require two-way coupling with a high-resolution model which could resolve such processes as described here. The skill of models to forecast waves in the Arctic is then crucially dependent on the accuracy of the ice forecast, requiring resolution of ice fields on time and space scales of hours and kilometers. In reality, operational implementation at such scales is not presently possible.

4.5. Climate Change?

Singular events cannot be attributed to long time scale processes such as climate change. So the question of whether or not this large wave event in Arctic ice is a consequence of a changing climate is ill posed. A better question is, will energetic wave events occur more frequently in the Arctic in the future as the climate warms? Our answer is yes, a warmer climate will, as one reviewer noted, lead to declining summer sea ice cover (and delayed freeze-up in the fall). While fetch in the Norwegian and Barents Sea has historically been available, the extent of ice-free regions has recently reached historic levels, and completely new fetches have been exposed in the Beaufort, Chukchi, and East Siberian Seas. Furthermore, there is evidence of increased storm activity in the Arctic [Sepp and Jaagus, 2011]. All of this effectively exacerbates the fetch-wave, wave-ice, ice-fetch feedback loop, and highly energetic wave events will occur more frequently [e.g., Dobrynin *et al.*, 2012; Khon *et al.*, 2014].

A few of the potential impacts of increased wave heights may be rerouting of shipping, damage to industrial platforms, and the loss of land in coastal communities to erosion. As interest, presence, and research in the Arctic intensifies, these observations are soon to be complemented by measurements of more and more energetic wave events.

5. Conclusions

An energetic wave event under significant ice cover in the Arctic was measured by *R/V Lance* on 2 and 3 May 2010 in the vicinity of Svalbard, Norway. The results indicate three distinct phases of ice-wave interaction. During phase 1, the waves are completely blocked and/or scattered by ice and a spectral wave model (without any ice representation) overpredicts the wave height, as expected. During phase 2, the ice was fractured by wave forcing and the fractured ice began to allow wave energy to propagate. This transition period lasted about an hour, during which time the waves appeared modulated or groupy. Modulation instability, hypothesized to be triggered by a change in wave dynamics in ice, is proposed as a possible mechanism for the initial breakup of ice. Firm conclusions were hindered by the lack of detailed ice properties and the speculative nature of the dispersion relationship in ice covered seas, but the authors regard this as a promising avenue for future research. During phase 3, the wave model and measurements were in excellent agreement, implying peak waves propagated through the ice uninhibited. The agreement continued over the course of 7 h during which time the measurements indicate an extension of allowed frequencies to those above the peak. Our results suggest that accurate wave prediction would have required coupling with an ice model which resolved scales of hours and kilometers. Implementation at such scales will no doubt be a future challenge. These are the largest known waves recorded in the Arctic with substantial ice cover present, and we expect the measurement of large-wave events to occur more frequently in the future due to the fetch wave-ice fetch feedback loop.

References

- Asplin, M. G., R. Galley, D. G. Barber, and S. Prinsenberg (2012), Fracture of summer perennial sea ice by ocean swell as a result of Arctic storms, *J. Geophys. Res.*, *117*, C06025, doi:10.1029/2011JC007221.
- Asplin, M. G., R. Scharien, B. Else, S. Howell, D. G. Barber, T. Papakyriakou, and S. Prinsenberg (2014), Implications of fractured Arctic perennial ice cover on thermodynamic and dynamic sea ice processes, *J. Geophys. Res. Oceans*, *119*, 2327–2343, doi:10.1002/2013JC009557.
- Babanin, A. V., and Y. P. Soloviev (1998), Field investigation of transformation of the wind wave frequency spectrum with fetch and the stage of development, *J. Phys. Oceanogr.*, *28*(4), 563–576.
- Benjamin, T. B., and J. Feir (1967), The disintegration of wave trains on deep water Part 1. Theory, *J. Fluid Mech.*, *27*(03), 417–430.
- Booij, N., R. C. Ris, and L. H. Holthuijsen (1999), A third-generation wave model for coastal regions: 1. Model description and validation, *J. Geophys. Res.*, *104*(C4), 7649–7666, doi:10.1029/98JC02622.

Acknowledgments

Many thanks to the captain and crew of the *R/V Lance*. Travis Smith helped with understanding the synoptic weather conditions. Ben Holt (NASA JPL) generously provided that satellite imagery used in Figure 1a and Figure S4 in the supporting information. We acknowledge the input from two anonymous reviewers whose comments increased quality and clarity of the manuscript. C.O.C. is supported by an ASEE postdoctoral fellowship at NRL-SSC. The support of ONR grants N0001413WX20825 and N000141310278 is acknowledged by W.E.R. and A.V.B., respectively. Raw shipborne data used in this study may be obtained by contacting coauthor A.M. by email: Aleksey.Marchenko@unis.no. The processed data used in the figures can be obtained by contacting the first author. Several open source MATLAB toolboxes were used during analysis and plotting including WAFO, MACE, j_lab, and M_Map.

The Editor thanks Matthew Asplin and an anonymous reviewer for their assistance in evaluating this paper.

- Campbell, A. J., A. J. Bechle, and C. H. Wu (2014), Observations of surface waves interacting with ice using stereo imaging, *J. Geophys. Res. Oceans*, *119*, 3266–3284, doi:10.1002/2014JC009894.
- Doble, M. J., and J. Bidlot (2013), Wave buoy measurements at the Antarctic sea ice edge compared with an enhanced ECMWF WAM: Progress towards global waves-in-ice modelling, *Ocean Modell.*, *70*, 166–173.
- Dobrynin, M., J. Murawsky, and S. Yang (2012), Evolution of the global wind wave climate in CMIP5 experiments, *Geophys. Res. Lett.*, *39*, L18606, doi:10.1029/2012GL052843.
- Fox, C., and T. G. Haskell (2001), Ocean wave speed in the Antarctic marginal ice zone, *Ann. Glaciol.*, *33*(1), 350–354.
- Fox, C., and V. A. Squire (1994), On the oblique reflexion and transmission of ocean waves at shore fast sea ice, *Proc. R. Soc. London, Ser. A*, *347*(1682), 185–218.
- Gol'dshtein, R. V., and A. V. Marchenko (1989), The diffraction of plane gravitational waves by the edge of an ice cover, *J. Appl. Math. Mech.*, *53*(6), 731–736.
- Hanson, K. A., T. Hara, E. J. Bock, and A. B. Karachintsev (1997), Estimation of directional surface wave spectra from a towed research catamaran*, *J. Atmos. Oceanic Technol.*, *14*, 1467–1482, doi:10.1175/1520-0426(1997)014<1467:EODSWS>2.0.CO;2.
- Hibler, W. D., III (1979), A dynamic thermodynamic sea ice model, *J. Phys. Oceanogr.*, *9*, 815–846, doi:10.1175/1520-0485(1979)009<0815:ADTSIM>2.0.CO;2.
- Hogan, T. F., and T. E. Rosmond (1991), The description of the Navy Operational Global Atmospheric Prediction System's spectral forecast model, *Mon. Weather Rev.*, *119*(8), 1786–1815.
- Hunkins, K. (1962), Waves on the Arctic Ocean, *J. Geophys. Res.*, *67*(6), 2477–2489, doi:10.1029/JZ067i006p02477.
- Janssen, P. A. E. M. (2003), Nonlinear four-wave interactions and freak waves, *J. Phys. Oceanogr.*, *33*(4), 863–884.
- Keller, J. B. (1998), Gravity waves on ice-covered water, *J. Geophys. Res.*, *103*(C4), 7663–7669, doi:10.1029/97JC02966.
- Khon, V. C., I. I. Mokhov, F. A. Pogarskiy, A. V. Babanin, K. Dethloff, A. Rinke, and H. Matthes (2014), Wave heights in the 21st century Arctic Ocean simulated with a regional climate model, *Geophys. Res. Lett.*, *41*, 2956–2961, doi:10.1002/2014GL059847.
- Kohout, A., M. Williams, S. Dean, and M. Meylan (2014), Storm-induced sea-ice breakup and the implications for ice extent, *Nature*, *509*(7502), 604–607.
- Liu, A. K., and E. Mollo-Christensen (1988), Wave propagation in a solid ice pack, *J. Phys. Oceanogr.*, *18*(11), 1702–1712.
- Liu, A. K., B. Holt, and P. W. Vachon (1991), Wave propagation in the marginal ice zone: Model predictions and comparisons with buoy and synthetic aperture radar data, *J. Geophys. Res.*, *96*(C3), 4605–4621, doi:10.1029/90JC02267.
- Marchenko, A. V., and K. I. Voliak (1997), Surface wave propagation in shallow water beneath an in-homogeneous ice cover, *J. Phys. Oceanogr.*, *27*, 1602–1613.
- Marko, J. R. (2003), Observations and analyses of an intense waves-in-ice event in the Sea of Okhotsk, *J. Geophys. Res.*, *108*(C93296), doi:10.1029/2001JC001214.
- Meylan, M. H., L. G. Bennetts, and A. L. Kohout (2014), In situ measurements and analysis of ocean waves in the Antarctic marginal ice zone, *Geophys. Res. Lett.*, *41*, 5046–5051, doi:10.1002/2014GL060809.
- National Geophysical Data Center (2006), U.S. Department of Commerce, National Oceanic and Atmospheric Administration, 2-minute Gridded Global Relief Data (ETOPO2v2). [Available at <http://www.ngdc.noaa.gov/mgg/fliers/06mgg01.html>]
- Newyear, K., and S. Martin (1999), Comparison of laboratory data with a viscous two-layer model of wave propagation in grease ice, *J. Geophys. Res.*, *104*(NC4), 7837–7840, doi:10.1029/1999JC900002.
- Perrie, W., and Y. Hu (1996), Air-Ice-Ocean momentum exchange. Part I: Energy Transfer between waves and ice floes, *J. Phys. Oceanogr.*, *26*, 1705–1720.
- Robin, G. D. Q. (1963), Wave propagation through fields of pack ice, *Proc. R. Soc. London, Ser. A*, *255*(1057), 313–339.
- Rogers, W. E., and M. D. Orzech (2013), Implementation and testing of ice and mud source functions in WAVEWATCH III® NRL/MR/7320–13-9462, 31 pp.
- Rogers, W. E., and S. Zieger (2014), S_{ice} : Damping by sea ice, in *User Manual and System Documentation of WAVEWATCH III(R) Version 4.18b*, edited by H. L. Tolman, pp. 60–61, NOAA/NWS, College Park, MD Tech. Note, MMAB Contribution 316.
- Sepp, M., and J. Jaagus (2011), Changes in the activity and tracks of Arctic cyclones, *Clim. Change*, *105*(3–4), 577–595.
- Squire, V. (2007), Of ocean waves and sea-ice revisited, *Cold Reg. Sci. Technol.*, *49*(2), 110–133.
- Squire, V. A., and T. B. Williams (2008), Wave propagation across sea-ice thickness changes, *Ocean Modell.*, *21*, 1–11.
- Squire, V. A., J. P. Dugan, P. Wadhams, P. J. Rottier, and A. K. Liu (1995), Of ocean waves and sea ice, *Annu. Rev. Fluid Mech.*, *27*(1), 115–168.
- Squire, V. A., G. L. Vaughan, and L. G. Bennetts (2009), Ocean surface wave evolution in the Arctic Basin, *Geophys. Res. Lett.*, *36*, L22502, doi:10.1029/2009GL040676.
- Thomson, J., and W. E. Rogers (2014), Swell and sea in the emerging Arctic Ocean, *Geophys. Res. Lett.*, *41*, 3136–3140, doi:10.1002/2014GL059983.
- Timco, G. W., and W. F. Weeks (2010), A review of the engineering properties of sea ice, *Cold Reg. Sci. Technol.*, *60*(2), 107–129, doi:10.1016/j.coldregions.2009.10.003.
- Tolman, H., and the WAVEWATCH III® Development Group (2014), User Manual and System Documentation of WAVEWATCH III® version 4.18, *Tech. Note 316*, NOAA/NWS/NCEP/MMAB, 282 pp.
- Tolman, H. L. (2003), Treatment of unresolved islands and ice in wind wave models, *Ocean Modell.*, *5*(3), 219–231.
- Tuomi, L., K. K. Kahma, and H. Pettersson (2011), Wave hindcast statistics in the seasonally ice-covered Baltic Sea, *Boreal Environ. Res.*, *16*(6), 451–472.
- Van Woert, M. L., C. Zou, W. N. Meier, P. D. Hovey, R. H. Preller, and P. G. Posey (2004), Forecast verification of the Polar Ice Prediction System (PIPS) sea ice concentration fields*, *J. Atmos. Oceanic Technol.*, *21*(6), 944–957.
- Wadhams, P. (1981), The ice cover in the Greenland and Norwegian Seas, *Rev. Geophys.*, *19*(3), 345–393, doi:10.1029/RG019i003p00345.
- Wang, R., and H. H. Shen (2010), Gravity waves propagating into an ice-covered ocean: A viscoelastic model, *J. Geophys. Res.*, *115*, C06024, doi:10.1029/2009JC005591.
- Yuen, H. C., and M. Lake (1982), Nonlinear dynamics of deep water gravity waves, *Adv. Appl. Mech.*, *22*, 67–229.